Final Draft

of the original manuscript

Fang, L.; Gould, O.E.C.; Lysyakova, L.; Jiang, Y.; Sauter, T.; Frank, O.; Becker, T.; Schossig, M.; Kratz, K.; Lendlein, A.:

Implementing and Quantifying the Shape-Memory Effect of Single Polymeric Micro/Nanowires with an Atomic Force Microscope.

In: ChemPhysChem. Vol. 19 (2018) 16, 2078 - 2084.

First published online by Wiley-VCH: 23.04.2018

https://dx.doi.org/10.1002/cphc.201701362

Full Paper

Implementing and Quantifying the Shape-Memory Effect of Single Polymeric Micro/Nanowires with an Atomic Force Microscope

Liang Fang, Oliver E.C. Gould, Liudmila Lysyakova, Yi Jiang, Tilman Sauter, Oliver Frank, Tino Becker, Michael Schossig, Karl Kratz, Andreas Lendlein *

Dr. Liang Fang, Dr. Oliver Gould, Dr. Liudmila Lysyakova, Yi Jiang, Dr. Tilman Sauter, Oliver Frank, Tino Becker, Michael Schossig, Dr. Karl Kratz, Prof. Andreas Lendlein.
Institute of Biomaterial Science, Helmholtz-Zentrum Geesthacht, Kantstr. 55, 14513 Teltow, Germany
E-mail: andreas.lendlein@hzg.de

Yi Jiang, Prof. Andreas Lendlein.
Institute of Chemistry, University of Potsdam, Karl-Liebknecht-Straße 24-25, 14476 Potsdam, Germany

Dr. Liang Fang.
Present Address: College of Materials Science and Engineering, Nanjing Tech University, Nanjing 210009, PR China

Dr. Tilman Sauter.
Present Address: Evonik Industries AG, Paul-Baumann-Str. 1, 45772 Marl, Germany

Abstract

The implementation of shape-memory effects (SME) in polymeric micro- or nano-objects currently relies on the application of indirect macroscopic manipulation techniques, e.g. stretchable molds or phantoms, to ensembles of small objects. Here, we introduce a method capable of the controlled manipulation and SME quantification of individual micro- and nano-objects in analogy to macroscopic thermomechanical test procedures. An atomic force microscope was utilized to address individual electro-spun poly(ether urethane) (PEU) micro- or nanowires freely suspended between two micropillars on a micro-structured silicon substrate. In this way, programming strains of 10 ± 1% or 21 ± 1% were realized, which could be successfully fixed. An almost complete restoration of the original free suspended shape

during heating confirmed the excellent shape-memory performance of the PEU wires. Apparent recovery stresses of $\sigma_{max,\ app}$ = 1.2 ± 0.1 and 33.3 ± 0.1 MPa were obtained for a single microwire and nanowire, respectively. The universal AFM test platform described here enables the implementation and quantification of thermomechanically induced function for individual polymeric micro- and nanosystems.

Keywords: cyclic thermomechanical testing, atomic force microscopy, soft matter micro- and nanowires, shape-memory effect, material science.

1. Introduction

The thermomechanical manipulation of polymers is a versatile method for implementing new functions such as shape-memory effects[1] or actuation capability into soft materials. Here, the precise control of applied parameters during thermomechanical manipulation is required to impart a desired functionality. For shape-memory materials a specific processing technology, named programming, seeks to exploit a polymer's molecular architecture/nanoscale structure to generate controlled physical motion. Through this thermomechanical treatment a shape-memory polymer (SMP) can be deformed and fixed into a temporary shape distinct from the permanent shape created by conventional polymer processing techniques. For a macroscale SMP specimen cyclic, thermomechanical tests, such as tensile, compression or three-point bending, have emerged as one of the most powerful methods to precisely control applied parameters necessary to implement SME function.[2] These methods enable the simultaneous control of physical parameters such as stress, strain and temperature in a single, fixed experimental setup as well as the measurement of their impact on certain shape-memory characteristics such as shape fixity ratio or switching temperature.

Recent work has successfully translated SME technology to micro/nanoscale objects where complex behaviors, such as multiple shape change[3–5] and reversible shape-memory effects,[6,7] have made shape-memory materials desirable for a range of biomedical[8–11] and micromechanical[12–20] applications. However, the translation of shape-memory materials into useful nano/micro technologies has relied on the simultaneous programming of large numbers of micro/nanostructures using structured surfaces or particle ensembles within a programming area spanning several millimeters or centimeters.[14,21,22] With such macroscopic ensemble programming methods control over the key parameters, which determine shape-memory function is severely limited. Further, the quantification of temperature-induced shape change has been mostly limited to the visualization of their recovery behaviors using various microscopy techniques.[8,10,20,21,23–27] To fully control the programming process, and to

comprehensively quantify the shape-memory behavior, a means of individually addressing a single micro/nano-object is necessary. Here, we have utilized an AFM cantilever to program and fix single, free-suspended micro/nanowires placed on a structured silicon substrate, to a temporarily bended shape. The capability of this method was demonstrated for an aliphatic polyether urethane (PEU) with a broad mixed glass transition ($T_{g,\,mix}$) ranging from 20 °C to 90 °C. This PEU was chosen for this study based on its excellent macroscopic SME properties,[28–30] its processability into micro- and nanowires using electrospinning,[31] and to eliminate crystallization related effects.

A typical shape-memory test protocol is shown schematically in Figure 1A. The programming process is typically accomplished with three steps. In the first step, the sample is cooled from T_{high} to a certain deformation temperature (T_{deform}), before undergoing elongation to a temporary shape ε_m. In our AFM-based testing process a peltier stage enables the accurate heating and cooling of the sample. The nano/microwire is "clamped" through attachment to two pillars on the structured silicon substrate, before three-point stretching by the cantilever causes elongation to a temporary deformed shape. To fix the temporary structure the sample is cooled to T_{low}, freezing the switching segments while ε_m is kept constant. In the final step the stress is released leaving the fixed temporary shape ε_u, which is accomplished in our method by withdrawing the cantilever.

For the recovery step, the sample is reheated to T_{high} causing it to revert to its original shape. Here, a macroscale tensile testing apparatus can either allow the material to recover with or without stress by generating a force against that of the SMP. To achieve stress recovery the AFM is used in contact mode, allowing the generation of a constant force against the nano/microwire during its recovery. To characterize simple shape recovery the AFM is used in AC mode, enabling the accurate measurement of the midpoint of the fiber during recovery without generating stress. Similar to a macroscopic testing apparatus, which allows for comprehensive testing on the same experimental setup, the deformation and shape/stress

recovery of programmed micro-/nanowires were all characterized in real-time using the same cantilever. A schematic illustration of microwire programming and recovery is displayed in Figure 1 B-D and E-G. This approach enables the measurement of key characteristic values such as strain fixity, recovery ratio and switching temperature, on the nano/microscale while implementing function by controlling parameters such as stress, strain and deformation temperature.

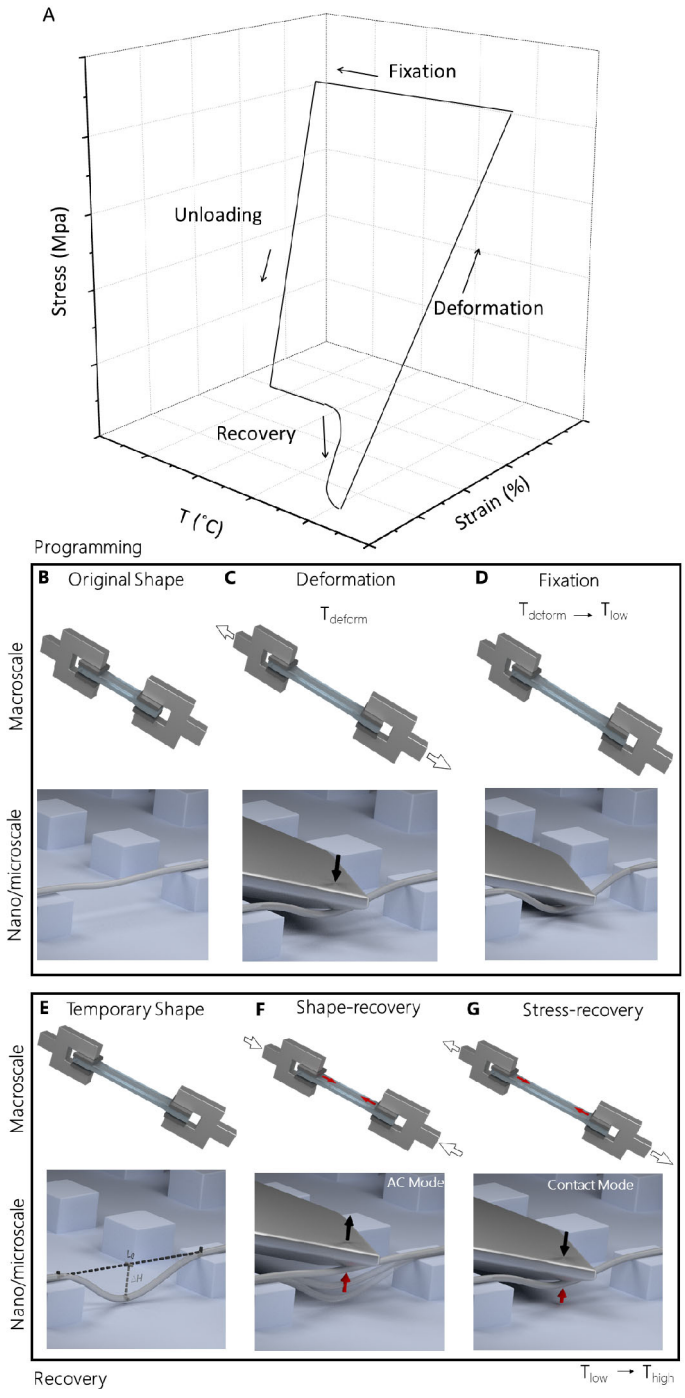

Figure 1. A) Schematic illustration of the stress-temperature-strain diagram obtained in macroscale shape-memory tests. B-D) Schematic of the vertical deformation and fixation process for a single PEU microwire. F,G) Schematic showing the shape (F) and stress (G) recovery of a deformed micro/nanowire. Each step in the programming and recovery process is shown with its macroscopic equivalent in a clamped tensile testing apparatus.

2. Results and Discussion

A micro-structured silicon wafer comprising cubic micro-pillars (with a height of 10.0 ± 0.1 µm and an inter-pillar spacing of 20.0 ± 0.1 µm) was used as a support for the microfibers. The heat transfer kinetics on this length scale, and specifically the effect on the actuation behaviour of the material, are relatively unknown. To accommodate for this silicon was chosen as the substrate material, as its high thermal conductivity should minimize its interference in heat transfer to the nano/microwires. The dimensions of the pillars were chosen to provide ample support for the microwires, to yield the highest number of parallel fibers during electrospinning, and to minimize contact between the cantilever and the pillars during deformation. The height of the pillars was chosen to prevent any adhesion between the bottom of the trench and the micro/nanowires.

PEU fibers with a diameter of approx. 1 µm were successfully deposited on top of the pillars by electrospinning, and imaged by scanning electron microscopy (SEM) (Figure 2A). To avoid any unwanted overall movement of the microfibers and to eliminate the fiber-substrate friction associated with the programming, the supporting parts of the fibers and the pillar top surfaces were glued together using a 1,1,1-3,3,3 hexafluoro-2-propanol vapor. To verify the successful adhesion of the microfiber, it was laterally deformed while kept at T_{deform} = 40 ºC and monitored using optical microscopy (as shown in Supplementary Figure 4). Nanowires with diameters of 98 ± 27 nm (as analysed by SEM) were electrospun onto ridges on a structured silicon wafer, spaced by 3 ± 0.1 µm with a groove depth of 1 ± 0.1 µm (Figure 2B).

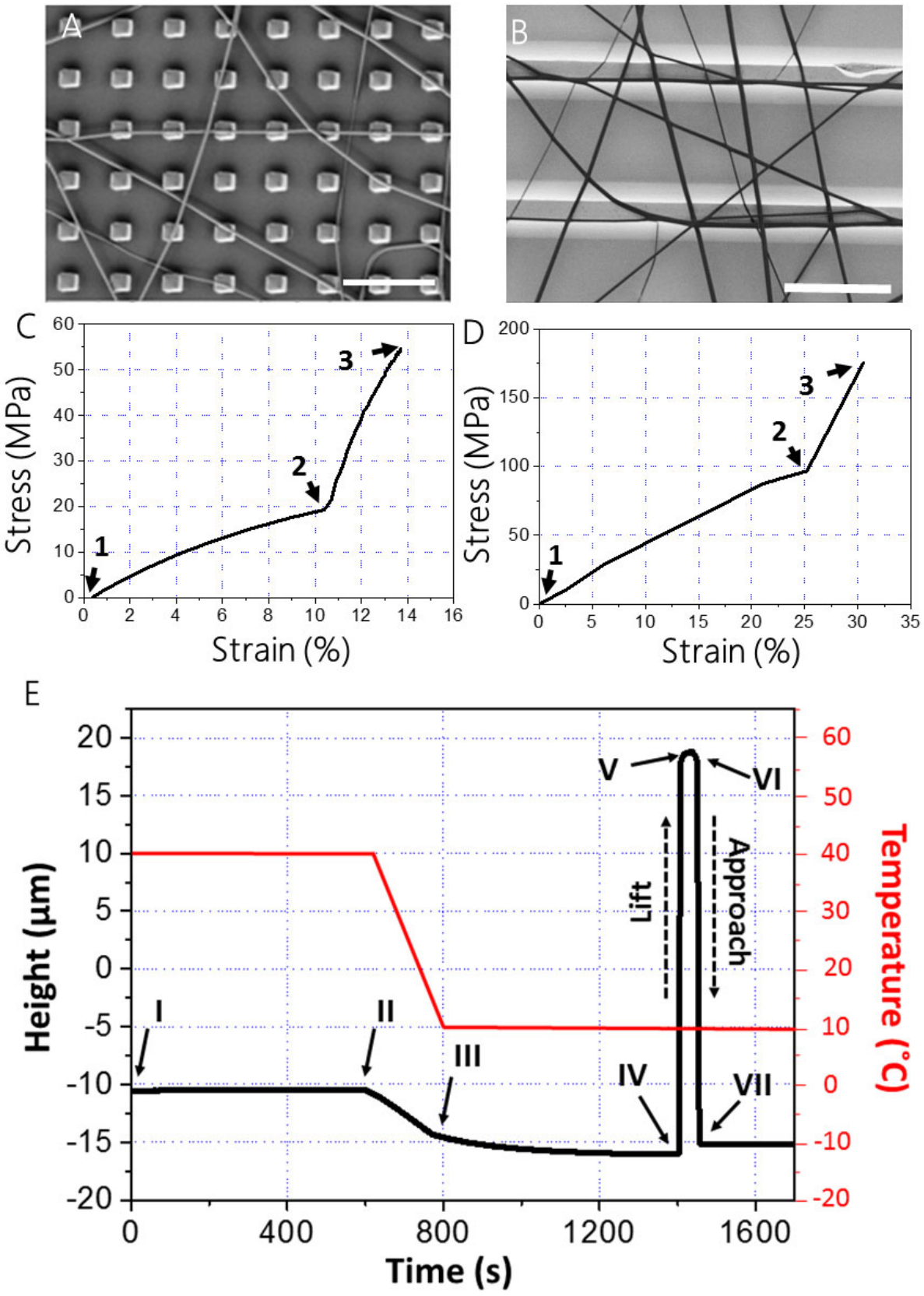

Figure 2. (A,B) Scanning electron microscopy images of the electrospun micro- and nanowires on structured wafers. The scale bars are (A) 50 μm and (B) 2 μm. C,D) Stress-strain curves of single (C) micro and (D) nanowires during programming by an AFM

cantilever in contact mode. Point 1 and 2 indicate the onset and the ending points of deforming the micro- and nanowires. Point 3 indicates the moment at which the approaching step ceased while the set point of the force was reached. (E) Characteristic real-time height (Z-piezo) curve given by the AFM during fixation. Point I-II: the deformation of the microwire was maintained at 40 ºC for 10 min to allow relaxation. Point II-III: the temperature was reduced from 40 to 10 ºC. Point III-IV: the deformed microwire was kept at 10 ºC for another 10 min. Point IV-V: the cantilever was withdrawn and returned back to its highest point. Point V-VI: the AFM mode was switched from contact to AC mode to enable the determination of the variation in the fixed height. Point VI-VII: the AFM cantilever was approached onto the microwire again.

2.1 Controlled Programming of Individual Micro/nanowires

Initial experiments aimed to demonstrate a microfiber's precise deformation and fixation using an AFM cantilever and temperature control. Firstly, the temperature of the testing system was cooled down from T_{high} = 80 ºC to T_{deform} using a Peltier element and equilibrated for 10 min. To allow for the targeting of a specific programming site, a single, free-standing PEU microwire (Figure 1B) was then imaged using AFM. After positioning, the cantilever was set to approach the wire axially in contact mode with a set force of 25 µN and an approach rate of 8.6 nm·s^{-1} (Figure 1C). The deformed wire was then equilibrated under load at T_{deform} for 10 min. Subsequent cooling of the microfiber to T_{low} = 10 ºC, while under constant strain from the cantilever, resulted in the fixation of the applied deformation (Figure 1D) and after withdrawing the cantilever the temporary deformed shape is obtained (Figure 1E). For this process, the same cantilever must be capable of obtaining a clear height image of the free-suspended polymeric wires, and of directing their controlled deformation. For the purpose of imaging, the tip of the cantilever should be sharp. However, a sharp tipped cantilever tended to slip from the curved microfiber surface and lose contact with the wire during the axial programming procedure. Therefore, a tip-less cantilever (Supporting Information Figure S1) was used for the cyclic, thermomechanical testing of the microwires at the loss of some image quality. Due to the spatial constraints of the substrate and cantilever the maximum deformation possible with this technique was limited to around 20% for the nanofiber setup and around 10% for the microfiber setup. The real-time monitoring of the

microfiber during programming was possible by measuring the deflection and height (Z-piezo) data collected by the AFM, whereby the background resulting from the thermal expansion/contraction of the test system needs to be subtracted for achieving the height values (Supporting Figure S2 and Figure 3). These could be used to calculate the actual stress (σ) experienced by the micro/nanowire and its associated strain (ε) according to the equations 1 and 2 (see Supporting Method S1 for the full calculation procedure).

$$\sigma = \frac{Def \cdot K}{\pi R^2} \cdot \frac{\sqrt{(\Delta H)^2 + (L_0/2)^2}}{\Delta H} \quad (1)$$

$$\varepsilon = \left(\sqrt{4(\Delta H/L_0)^2 + 1} - 1\right) \times 100\% \quad (2)$$

Here, *Def* is the real-time deflection data of the cantilever collected by the AFM, *K* stands for the spring constant value of the cantilever, *R* is the radius of the micro- /nanowire, ΔH is the real-time height variation of the wire midpoint, collected by AFM, L_0 is the initial length of the micro-/nanowire during the programming.

The obtained stress-strain curves for the deformation of a single microwire and nanowire at 40 °C is shown in Figure 2C. The stress increased almost linearly as the microwire was loaded (point 1 - 2) until a maximum value of σ_m = 19 ± 2 MPa and ε_m = 10 ± 1%. Here, an obvious inflection point was observed (point 2) suggesting that the flanks of the tip-less cantilever had come into contact with the edges of the supporting silicon pillars, resulting in the applied force acting on the pillars instead of further deforming the microwire (point 2 - 3). When the set point of the force was reached (point 3) the programming was complete. The elastic modulus of the microwire at T = 40 °C was calculated as E_{micro} =186 ± 20 MPa, which is comparable to that of bulk PEU materials (E_{bulk} = 206 ± 20 MPa).[1]

Since the height image given by a tip-less cantilever does not allow an accurate measurement of the microwire height, the real-time height curve (Figure 2E) was used to determine its

remaining strain (ε_u) in the N^{th} test cycle and the strain fixity ratio R_f according to equation 3, where ε_m is the deformation strain.

$$R_f(N) = \frac{\varepsilon_u(N)}{\varepsilon_m} \times 100\% \quad (3)$$

A small height difference of 0.80 ± 0.05 µm was measured between the withdrawal of the cantilever and after the re-approach in AC mode, which could be attributed to a height variation of the microwire after releasing the load. This fixed height variation of the microwire enabled the calculation of the remaining strain as ε_u = 9.7 ± 0.1%, giving a strain fixity ratio of R_f = 93 ± 2 %.

To show the capability of our approach, and its applicability to nanoscale materials, we also demonstrate the controlled programming of PEU nanowires. A sharp-tipped cantilever (Supporting Information Figure S1) was used to enable the accurate positioning of the cantilever on the nanowires, and to prevent premature contact with the edges of the ridges. The maximum stress and strain of the nanowire during deformation, obtained from the stress-strain curve in Figure 2D, was typically around σ_m = 88 ± 2 MPa and ε_m = 21 ± 1%, yielding an elastic modulus of 415 ± 20 MPa. The height change of the midpoint of the nanowire was measured as approx. 1.0 ± 0.1 µm. As this value was close to the groove depth, it seems likely that the cantilever (length = 14 µm) reached the underlying groove surface, leading to an inflection point in the stress-strain curve (point 2, Figure 2D).

To characterize the programmed fibers, the AFM was switched from contact mode to AC mode allowing the cantilever to approach the microwire without applying considerable force. An AC-mode scan was performed to characterize the temporary shape at T_{low} = 10 °C. As shown in Figure 3C,D after the programming and fixing procedures, individual free-standing PEU microwires and nanowires were successfully vertically deformed and fixed in their temporary shape by the cantilever. The success of the programming and shape recovery process for the PEU nanowires was determined by comparing the heights of the fiber and its

surroundings. For example, the height difference between the silicon groove and the midpoint of the programmed PEU nanowire, as measured by AC-mode AFM, was used to calculate the remaining strain (ε_u). The similarity of the two values indicated that the temporary shape of the nanowire was completely fixed, i.e. the fixity ratio of nanowires $R_f = 100 \pm 2\%$.

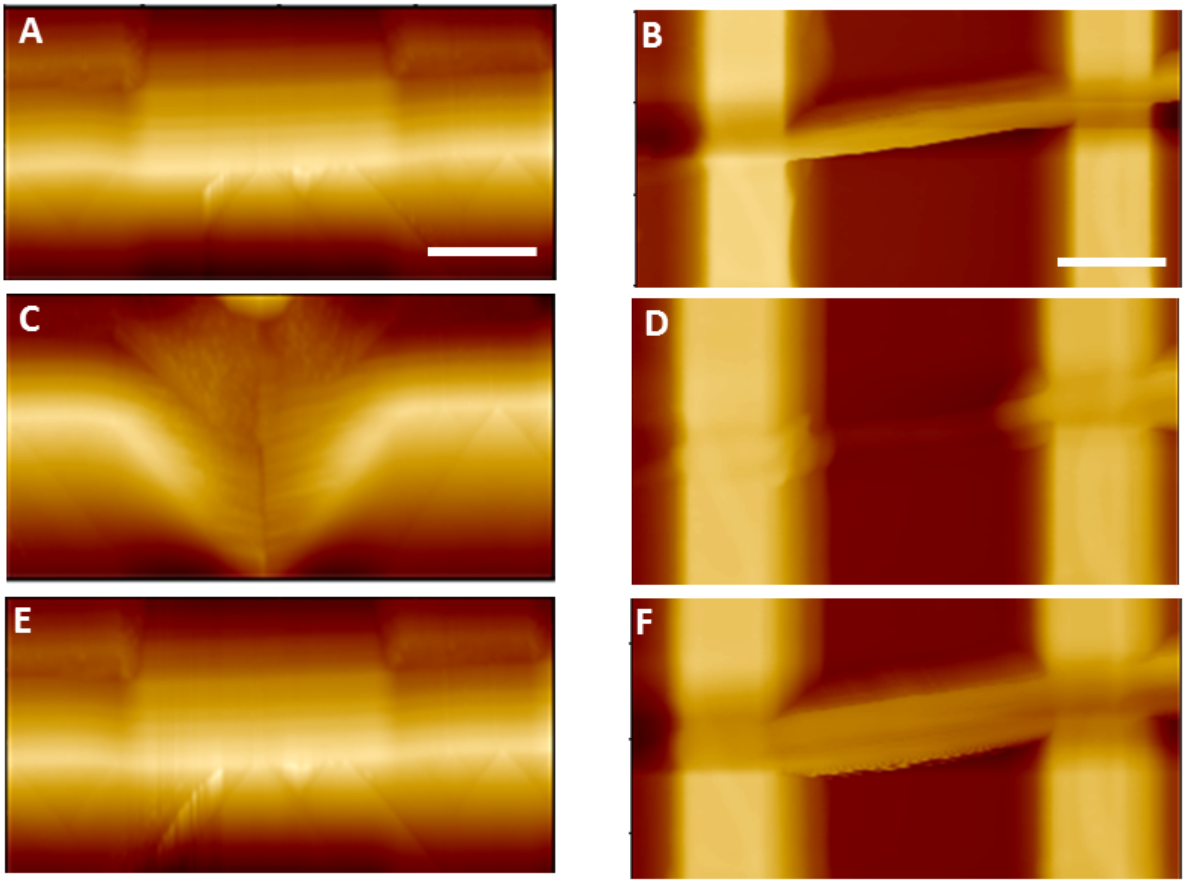

Figure 3. A,B) AFM height images of single, free-suspended (A) micro and (B) nanowires taken before the programming procedures at T_{deform} = 40 °C and T_{deform} = 30 ºC respectively. (C, D) AFM height images of the (C) micro and (D) nanowire in their temporary shape taken at T_{low} = 10 ºC. (E, F) AFM height images of these (E) micro and (F) nanowire after shape recovery. The scale bars for (A,C,E) microwire (B,D,F) nanowire are 8 µm and 1.2 µm respectively.

2.2 Quantification of Thermally-triggered Shape and Stress Recovery

The AFM's AC-mode enabled the characterization of the vertically deformed microfibers during the shape recovery process. After imaging the fixed microwire at 10 ºC (Figure 3C), the cantilever was withdrawn and repositioned at it's midpoint. With the scan size set to zero the cantilever maintained its position (the midpoint of the wire) in the AC-mode during the

wire's heat-induced recovery, detecting its height variation while only applying a negligible force.

During this measurement the height of the whole testing system also increased due to its thermal expansion with increasing temperature. To compensate for this, the ambient height variation of the system across the temperature range of the recovery was measured and subtracted (Supporting Information Figure S2).

In a three cyclic shape recovery experiment (heating from T_{low} = 10 to T_{high} = 80 ºC) of a microwire deformed at T_{deform} = 40 °C no obvious variation in the height was observed when the temperature was increased from 10 to 35 ºC. At approximately 35 ºC, the height of the microwire started to increase, reaching a maximum value of around 4.5 ± 0.2 µm at 62 ± 1 ºC. The recovery behavior of the microwire was found to be almost identical in all three repetitively test cycles (Supporting Information Figure S3).

$$R_r(N) = \frac{\varepsilon_u(N) - \varepsilon_p(N)}{\varepsilon_u(N) - \varepsilon_p(N-1)} \times 100\% \quad (4)$$

The strain recovery ratio R_r can be calculated by equation 4, where ε_p is the elongation obtained after recovery at T_{high}. The final height of the microwire after recovery (at T_{high} = 80 ºC) was usually higher than its pre-programmed height (measured at T = 40 ºC) due to its thermal expansion. Since the strain incurred in the programming process was relatively small, limited by the pillar and cantilever geometry, the strain recovery ratio (R_r) of the microwire can be considered as 100%. The complete recovery of the programmed microwire is also shown in Figure 3E, showing the AFM height image of one single microwire after shape recovery.

The switching temperature, T_{sw} = 54 ± 1 ºC, which represents the value, at which the maximum shape change occurred, was determined from the inflection point in the height-temperature curve in Figure 4 for T_{deform} = 40 ºC. The dependence of T_{sw} on the deformation temperature (T_{deform}) is also demonstrated in Figure 4. The height variations of the same

programmed PEU microwire during multiple shape recoveries, where T_{deform} was varied between 30 and 70 ºC, show that the switching temperature T_{sw} increases from T_{sw} = 53 ± 1 ºC at T_{deform} = 30 ºC to T_{sw} = 63 ± 1 ºC at T_{deform} = 70 ºC, while R_r was not affected. These findings are in good agreement with the reported variation in T_{sw} of PEU bulk samples when the deformation temperature was changed from 25 to 70 °C.[30]

The direct measurement of the nanowire's height variation during shape recovery was prevented by the nanowire's high tendency to break while being probed in AC-mode. This limitation could potentially be overcome by replacing the cantilever with a gentler colloidal probe-based measurement system. This would also be necessary to realize the deformation and recovery characterization of smaller diameters of nanowire. The recovery ratio R_r was calculated by comparing the height difference between the nanowire surface and the flat ridge area. As shown in Figure 3B and F, this did not vary considerably before programming and after recovery, suggesting a complete shape recovery, i.e. R_r = 100%.

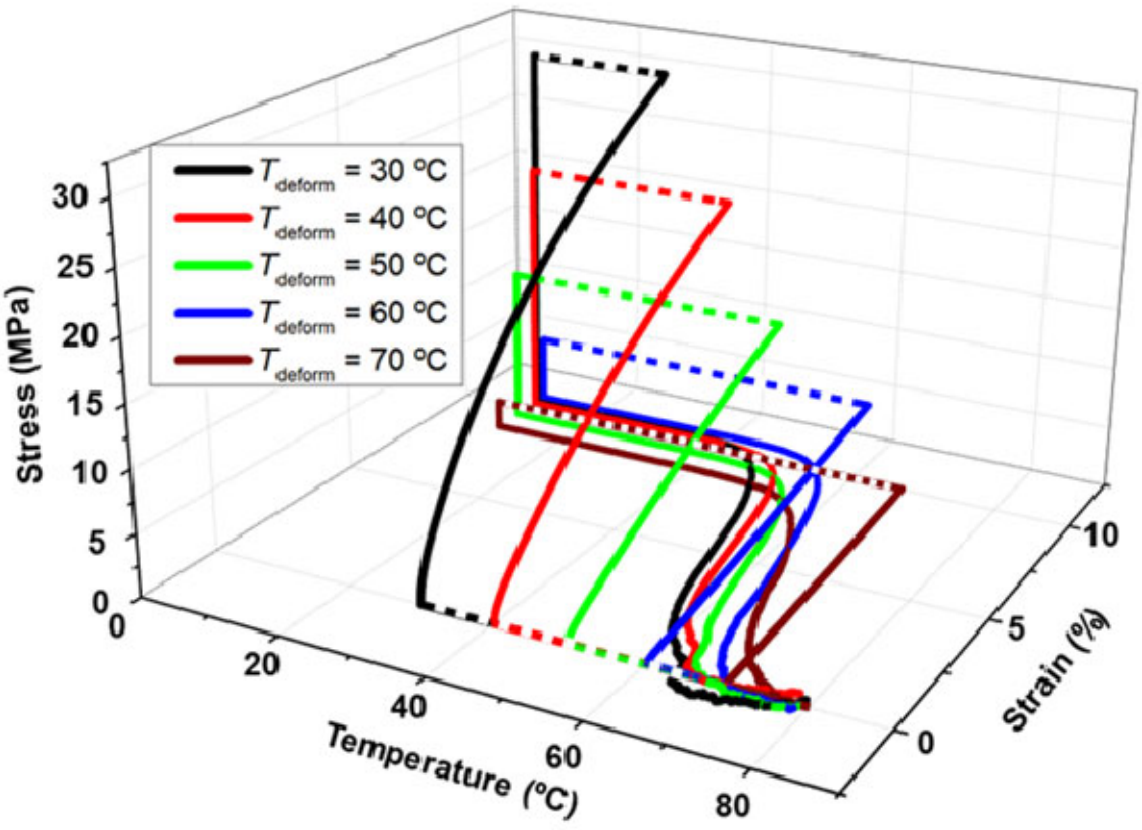

Figure 4. Stress-temperature-strain diagram of a single microfiber during the shape recovery at a T_{deform} of 30, 40, 50, 60 and 70 ºC. Here solid lines indicate where stress-temperature-strain data was simultaneously obtained.

2.2.1 Stress Recovery of PEU Micro- and Nanofibers

The use of contact mode during the recovery process enables the quantification of the stress recovery of the microwires. During the restoration of its original shape, the microwire generates a specific force outwards against the cantilever, resulting in a deviation from the set force.

Figure 5A shows a comprehensive AFM-mediated stress-temperature-strain plot obtained under stress recovery of an individual free-standing PEU microwire programmed at T_{deform} = 40 °C. The low deformation temperature of 40 °C was chosen, as here a large recovery stress (σ_{max}) can be expected. According to a previous report[30] about PEU bulk samples deformed to elongations ≥ 150% in such a cold drawing like deformation scenario the σ_{max} values are typically 60% of the applied deformation stress (σ_m). Step 1 in the stress-temperature-strain diagram represents cooling of the wire from T_{high} = 80 °C to T_{deform} = 40 °C. Afterwards the sample is deformed to ε_m (Step 2) finally reaching σ_m = 27 ± 0.1 MPa and subsequently cooled to T_{low} = 10 °C (Step 3). The temporary shape represented by ε_u is obtained after the stress was released (Step 4). Stress recovery is achieved by reheating the programmed microwire to T_{high} = 80 °C. During the stress recovery, a slight increase in the stress with increasing temperature was observed due to the thermal expansion of the whole test system. In addition, due to the increased heating rate, the switch from cooling to heating by the Peltier element was earlier, creating an artifact between 17 and 27 ºC. At around 68 ºC, an increase in the stress was observed, with a maximum value of 4.6 ± 0.1 MPa seen at approx. 75 ± 1 ºC. The apparent maximum recovery stress $\sigma_{max, app}$ = 1.2 ± 0.1 MPa, could be determined as the difference between the maximum stress and the stress at which the recovery peak started, as

determined from the stress-temperature curve. The recovery of the wire (Step 6) by releasing the stress completes the stress recovery test cycle.

Finally, the stress recovery behavior of the PEU nanowires was investigated. As shown in Figure 5B, at T_{deform} = 30 ºC an increase in the stress was observed upwards of 67 ºC indicating the generation of a recovery force against the cantilever. The apparent maximum recovery stress $\sigma_{max,\ app}$ = 33.3 ± 0.1 MPa was determined as the difference between the maximum stress and the stress at which the recovery peak started. Interestingly, when the measurement was performed with T_{deform} at 40 and 50 ºC, this increase in stress was observed at 69 and 71 ºC. Although the T_{sw} cannot be measured accurately due to the high heating rate, this slight increase in the measured stress could indicate the onset of a temperature dependent behavior effect in the nanofilaments. When T_{deform} was 40 ºC, the maximum stress of 184.6 ± 0.1 MPa was found at around 74 ºC, while the apparent maximum recovery stress $\sigma_{max,\ app}$ = 33.3 ± 0.1 MPa was determined as the difference between the maximum stress and the stress, at which the recovery peak started.

Comparing the SMEs of the nano and microwires indicates that the recovery ratio is independent of wire scale, while the recovery stress of the nanowires (33.3 ± 0.1 MPa) is substantially larger than that generated by microwires (1.2 ± 0.1 MPa) or microfiber based non-wovens (0.7 ± 0.1 MPa).[31] We attribute this to a higher degree of orientation of the switching chain segments in the more confined dimensions of the nanowire, resulting in a higher mechanical resistance upon loading and recovery. To support this, future work will target the investigation of a wider range of wire diameters and also investigate the molecular orientation within the micro/nanowires using x-ray scattering. By combining the mechanical data measured here with nanoscale structural information, the investigation of key structural changes and their influence on physical function should be possible.

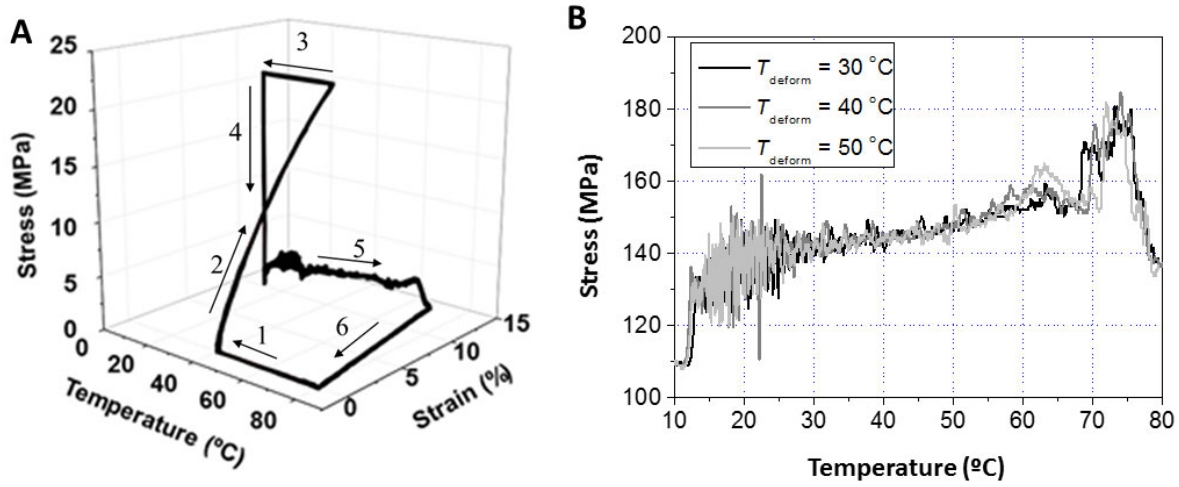

Figure 5. (A) Stress-temperature-strain plots at stress recovery conditions for a PEU microwire at a T_{deform} of 30 ºC. (D) Stress-temperature curves of nanowires obtained during stress recoveries. T_{deform} was 30, 40, and 50 ºC, respectively. n: cycle number.

3. Conclusion

Here, an AFM based method was introduced, which allows the cyclic, thermomechanical testing of single, independent PEU micro- and nanowires, enabling the implementation and quantification of a shape-memory function. The test set-up enabled the application of a programming strain of 10 ± 1% to microwires, while nanowires could be deformed to 21 ± 1%. The real-time quantification of PEU microwire's shape recovery resulted in high strain fixity ratios between 93% and 100% associated with a complete shape recovery, whereby the switching temperature could be adjusted from 53 to 63 ºC by varying the deformation temperature from 30 to 70 ºC. Stress recovery experiments allowed the analysis of the maximum recovery stress while heating the programmed wires to 80 °C. The microwires displayed a recovery stress of 1.2 MPa, while the nanowires were able to reach 33.3 ± 0.1 MPa. This novel AFM-based method enables the thermomechanical manipulation and quantification of single polymeric wires at the micro- and nanoscale, which is expected to significantly aid the implementation and characterization of more complex actuation behaviors such as multiple shape change. This work provides a platform for the translation of

polymeric materials into useful nano/micro technologies by demonstrating comprehensive experimental micro- or nanoscale characterization of mechanical behavior in analogy to cyclic, thermomechanical procedures used for characterization of macroscopic polymer specimens.

4. Experimental Section

Materials. Aliphatic PEU (trade name Tecoflex®, EG72D) was purchased from Noveon (Wilmington, MA, USA) and used without further purification.

Electrospinning. Micro- and nanowires were prepared according to the method described in Ref [31]. The aliphatic PEU was dissolved in 1,1,1-3,3,3 hexafluoro-2-propanol (HFP, ABCR GmbH, Karlsruhe, Germany) and formic acid (FA, Sigma Aldrich, St. Louis, MO, USA). Two different solutions were prepared by dissolving the PEU at ambient temperature; a PEU/HFP solution with 8% w/v and a PEU/HFP-FA (75/25 v/v) solution with 4% w/v. The electrospinning setup consisted of a 20 mL syringe, which was connected to a syringe pump. A metallic needle at the tip of the syringe served as hot electrode and a slowly rotating mandrel was used as collecting electrode. Electrospinning was conducted with around 1 $kV \cdot cm^{-1}$ and 1 $mL \cdot h^{-1}$. The supporting structured silicon wafers (IMS Chips, Stuttgart, Germany) were fixed in the spinning shadow of the mandrel by a conductive double-sided tape for the electrospinning process to equilibrate for 5 min. Subsequently, the supporting wafers were rotated towards the wire deposition and held there for several seconds. PEU microwires were deposited onto a silicon wafer with a periodic array of cubic micropillars with a length of 10.0 ± 0.1 μm, and the interpillar gap distance of 20.0 ± 0.1 μm. For the deposition of PEU nanowires, a silicon wafer with groove-ridge structures, where the distance between two ridges was 3 ± 0.1 μm and the groove depth was 1 ± 0.1 μm, was used.

To avoid an overall movement of the microwires and to eliminate the wire-substrate friction associated with the programming, it was necessary to glue the supporting parts of the wires and the pillar top surfaces together. Hence, the microwire covered wafer was stored for 5 min

in a desiccator filled with 30 mL HFP vapor. It was observed via SEM that a lateral movement of the AFM cantilever did not vary the wire positions on the top of the pillars, suggesting a firm attachment of the microwires onto the pillars.

Atomic Force Microscope (AFM). The cyclic, thermomechanical tests were performed by a MFP-3D AFM (Asylum Research). The temperature was controlled by an Environmental Controller (Asylum Research) with a Peltier element. Non-coated silicon cantilevers were utilized to avoid thermal expansions existing in the metal coating layers and thus prevent considerable temperature-dependent deflection of the cantilever itself. The silicon tip-less cantilevers (Nanosensors, TL-NCL-10) had a driving frequency of around 190 kHz and a spring constant of 79 $N \cdot m^{-1}$. The silicon sharp-tip cantilevers (Olympus OMCL, AC240TN, length = 14 μm, nominal radius = 7 nm) had a driving frequency of 66-88 KHz and a spring constant of 5 $N \cdot m^{-1}$. The AFM height images of the micro- and nanowires were obtained using tip-less or sharp-tip cantilevers, respectively, at the typical scanning rate of 1.0 Hz.

Programming and Fixation. The typical procedures for the microwires are described here as an example. The temperature of the testing system was cooled down from 80 ºC to T_{deform} = 70 or 60 or 50 or 40 or 30 °C and equilibrated for 10 min. After the cantilever has been placed to the midpoint of the microwire, it was approached onto the wire with a set force of 25 μN and an integral gain of 0.01, and accordingly a low approaching rate (8.6 $nm \cdot s^{-1}$). The real-time deflection and height (Z-piezo) data were simultaneously collected by the AFM. The microwire's deformation was kept for 10 min at 40°C before the temperature was reduced down to 10 ºC at 20 $ºC \cdot min^{-1}$ and equilibrated for another 10 min. Finally, the cantilever was lifted to release the load. To achieve a tight contact between the sharp tip and the wire curvature surface, the integral gain was set as high as 10 during the programming step, correspondingly the approaching rate was chosen (> 42.9 $\mu m \cdot s^{-1}$), and the equilibration time was 5 min. Also, the cooling-induced retraction of the testing system induced the downward movement of the cantilever to maintain its contact with the wire, generating a height

difference of 3.80 ± 0.05 μm prior to the fixation step. For the nanowires the set force was 500 nN. The stress-strain curves shown in Figure 2C,D were obtained for a single micro/nanowire undergoing a single programing procedure. Multiple wires of similar sizes were also tested to verify that the displayed data were representative.

Shape and Stress Recovery. To characterize the shape recovery, the AFM mode was switched from contact mode to AC mode prior to approaching the tip onto the midpoint of the temporarily deformed microwire. After the scan size and integral gain were set as 0 and 0.01, the temperature was increased from 10 to 80 ºC at a heating rate of 5 ºC·min^{-1}. The real-time height data were collected by AFM. For stress recovery, in AFM contact mode with the set force of 500 nN, the control speed of the system was decreased by setting a low integral gain of 0.01 to enhance the detection of the cantilever deflection deviation. After approaching the tip onto the midpoint of the temporarily deformed micro- / nanowire using AFM contact mode, the temperature was increased from 10 to 80 ºC at a high heating rate of 20 ºC·min^{-1}, while the real-time height (Z-piezo) data were collected by AFM. It is worth mentioning that in contrast to microwires, a significantly higher integral gain and thus approaching rate were applied in the programming of nanowires in order to achieve a tight contact between the sharp tip and the wire curvature surface. Also, the nanowire deformation took place over a shorter period.

Consecutive cyclic testing was however limited to two cycles on the same nanowire because of two reasons. (i) Even though the integral gain was set to the high value of 10.0, the tip still sometimes slipped away from the sharp tip during programming. (ii) The nanowire possessed a high tendency to break during the non-contact mode scanning or the programming step. Therefore, where necessary the repeated quantification of SMEs in nanowires was realized on different nanowires with similar geometry. Due to the small size of nanowires and related challenges in maintaining contact between their surface and the cantilever's tip, a complete real-time height-temperature curve could not be obtained for the nanowires. While the stress-

temperature-strain curves shown in Figure 4, 5 were obtained for a single micro/nanowire, multiple wires of similar sizes were also tested to verify that the displayed data for the recovery process were representative.

Supporting Information

Supporting Information is available from the Wiley Online Library or from the author.

Acknowledgement

This work was supported by the Helmholtz-Association through programme-oriented funding.

References

[1] M. Behl, M. Y. Razzaq, A. Lendlein, *Adv. Mater.* **2010**, *22*, 3388.

[2] T. Sauter, M. Heuchel, K. Kratz, A. Lendlein, *Polym. Rev.* **2013**, *53*, 6.

[3] S. M. Brosnan, A. M. S. Jackson, Y. Wang, V. S. Ashby, *Macromol. Rapid Commun.* **2014**, *35*, 1653.

[4] M. Farhan, T. Rudolph, U. Nöchel, W. Yan, K. Kratz, A. Lendlein, *ACS Appl. Mater. Interfaces* **2017**, *9*, 33559.

[5] Q. Ge, A. H. Sakhaei, H. Lee, C. K. Dunn, N. X. Fang, M. L. Dunn, *Sci. Rep.* **2016**, *6*, 31110.

[6] M. Behl, K. Kratz, J. Zotzmann, U. Nöchel, A. Lendlein, *Adv. Mater.* **2013**, *25*, 4466.

[7] T. Chung, A. Romo-Uribe, P. T. Mather, *Macromolecules* **2008**, *41*, 184.

[8] K. A. Davis, K. A. Burke, P. T. Mather, J. H. Henderson, *Biomaterials* **2011**, *32*, 2285.

[9] M. Ebara, *Sci. Technol. Adv. Mater.* **2015**, *16*, 14804.

[10] B. S. Lee, H. S. Shin, K. Park, D. K. Han, *J. Mater. Sci. Mater. Med.* **2011**, *22*, 507.

[11] W. Li, T. Gong, H. Chen, L. Wang, J. Li, S. Zhou, *RSC Adv.* **2013**, *3*, 9865.

[12] T. Meier, J. Bur, M. Reinhard, M. Schneider, A. Kolew, M. Worgull, H. Hölscher, *J.*

Micromechanics Microengineering **2015**, *25*, 65017.

[13] F. Zhang, Z. Zhang, T. Zhou, Y. Liu, J. Leng, *Front. Mater.* **2015**, *2*, 1.

[14] H. Xu, C. Yu, S. Wang, V. Malyarchuk, T. Xie, J. A. Rogers, *Adv. Funct. Mater.* **2013**, *23*, 3299.

[15] E. Lee, M. Zhang, Y. Cho, Y. Cui, J. Van Der Spiegel, N. Engheta, S. Yang, *Adv. Mater.* **2014**, *26*, 4127.

[16] M. Ebara, K. Uto, N. Idota, J. M. Hoffman, T. Aoyagi, *Soft Matter* **2013**, *9*, 3074.

[17] J. D. Eisenhaure, T. Xie, S. Varghese, S. Kim, *ACS Appl. Mater. Interfaces* **2013**, *5*, 7714.

[18] N. García-Huete, J. M. Cuevas, J. M. Laza, J. L. Vilas, L. M. León, *Polymers (Basel).* **2015**, *7*, 1674.

[19] M. Ebara, K. Uto, N. Idota, J. M. Hoffman, T. Aoyagi, *Adv. Mater.* **2012**, *24*, 273.

[20] Y. Zhao, W. M. Huang, Y. Q. Fu, *J. Micromechanics Microengineering* **2011**, *21*, 67007.

[21] C. Wischke, M. Schossig, A. Lendlein, *Small* **2014**, *10*, 83.

[22] Q. Zhang, T. Sauter, L. Fang, K. Kratz, A. Lendlein, *Macromol. Mater. Eng.* **2015**, *300*, 522.

[23] C. C. Fu, A. Grimes, M. Long, C. G. L. Ferri, B. D. Rich, S. Ghosh, S. Ghosh, L. P. Lee, A. Gopinathan, M. Khine, *Adv. Mater.* **2009**, *21*, 4472.

[24] Z. Wang, C. Hansen, Q. Ge, S. H. Maruf, D. U. Ahn, H. J. Qi, Y. Ding, *Adv. Mater.* **2011**, *23*, 3669.

[25] Y. Jiang, L. Fang, K. Kratz, A. Lendlein, *MRS Adv.* **2016**, *1*, 1985.

[26] L. M. Cox, X. Sun, C. Wang, N. Sowan, J. P. Killgore, R. Long, H. A. Wu, C. N. Bowman, Y. Ding, *ACS Appl. Mater. Interfaces* **2017**, *9*, 14422.

[27] L. M. Cox, J. P. Killgore, Z. Li, R. Long, A. W. Sanders, J. Xiao, Y. Ding, *Langmuir* **2016**, *32*, 3691.

[28] J. Cui, K. Kratz, M. Heuchel, B. Hiebl, A. Lendlein, *Polym. Adv. Technol.* **2011**, *22*, 180.

[29] T. Sauter, K. Lutzow, M. Schossig, H. Kosmella, T. Weigel, K. Kratz, A. Lendlein, *Adv. Eng. Mater.* **2012**, *14*, 818.

[30] J. Cui, K. Kratz, A. Lendlein, *Smart Mater. Struct.* **2010**, *19*, 65019.

[31] T. Sauter, K. Kratz, A. Lendlein, *Mater. Res. Soc. Symp. Proc.* **2012**, *1403*, 105.

Table of contents entry

Liang Fang, Oliver E.C. Gould, Liudmila Lysyakova, Yi Jiang, Tilman Sauter, Oliver Frank, Tino Becker, Michael Schossig, Karl Kratz, Andreas Lendlein *

Implementing and Quantifying the Shape-Memory Effect of Single Polymeric Micro/Nanowires with an Atomic Force Microscope

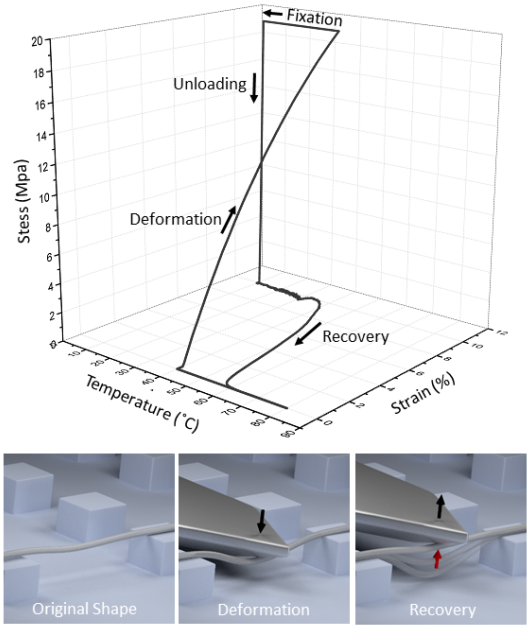

Comprehensive stress-temperature-strain curves for an individual microwire programmed at 40 °C and characterized by AFM during shape recovery. Schematic showing the deformation and quantification of the shape recovery of a polymeric microwire. The universal AFM test platform described here enables the implementation and quantification of thermomechanically induced function for various individual polymeric micro- and nanosystems.